HTML ABSTRACT + LINKS

High-field microwave effective linewidth in polycrystalline ferrites: Physical origins and intrinsic limits

Nan Mo,[a] Young-Yeal Song, and Carl E. Patton
Department of Physics, Colorado State University, Fort Collins, Colorado 80523

(Received 21 December 2004; accepted 15 February 2005; published online 14 April 2005)

High-precision high-field effective (HFE) linewidth measurements have been made at 10 GHz on ultradense hot isostatic pressed and conventionally sintered (CS) yttrium iron garnet ferrite materials. The accuracy was increased ten-fold relative to previous data through the use of a high-quality cavity, a modified measurement technique, and a fine adjustment of the gyromagnetic ratio based on the field-frequency response of the loaded cavity. The HFE linewidths for fields well above the region of degenerate bulk spin-wave band decreases with increasing field and extrapolates to known intrinsic single-crystal linewidths in the extreme high-field limit. From a field point shifted up from the high-field band edge dependent on degenerate dipole-exchange spin waves by $2/3$ the saturation induction, the data track closely the computed density of states for electromagnetic spin waves. In the case of the CS material, for fields below this point, one sees a microstructure-related increase related to conventional moderate wave number bulk-band spin waves. © *2005 American Institute of Physics*. [DOI: 10.1063/1.1887834]

I. INTRODUCTION

For over three decades, effective linewidth measurements have been used to characterize the resonance, near-resonance, and off-resonance losses in a wide range of polycrystalline ferrite materials.[1–10] The effective linewidth parameter ΔH_{eff}, in itself, provides a field-dependent loss parameter that reveals the details of the coupling between the driven mode, typically the uniform ferromagnetic resonance (FMR) mode, and the degenerate spin waves.

The recent resurgence of interest in spin dynamics and relaxation processes in magnetic systems[11–20] has motivated an examination of the effective linewidth and the related off-resonance losses in ferrites. The aim of this effort is to resolve some of the long standing questions about the fundamental loss processes in magnetic systems. This paper is concerned specifically with the losses at high fields that are well above the FMR field. These results should find applications for microwave and millimeter-wave devices as well as magnetic information storage systems.

For most ferromagnetic and ferrimagnetic systems, there is a relatively narrow range of field, typically called the "manifold region," for which the driven FMR mode is degenerate with moderate wave number (k) spin waves with micron wavelengths. In polycrystalline samples, the coupling to these spin-wave modes, termed "two-magnon scattering," usually dominates the relaxation. Following the early work of Schlömann,[21] Sparks,[22] and others, these manifold region two-magnon processes are reasonably well understood.

At high field, the situation is different. Here, the moderate- k spin-wave band is shifted up in frequency, there are typically no moderate- k spin waves degenerate with the pumping frequency, the two-magnon scattering contribution to the losses is disallowed, and the relaxation rate for the far-off-resonance driven mode should be field independent, small, and on the order of single-crystal linewidths. This is why the high-field effective (HFE) linewidth has typically been taken as a measure of the intrinsic losses, even in highly inhomogeneous ferrite materials. This is not the case found experimentally, however. Even though it is usually much smaller than typical FMR linewidths, the HFE linewidth in polycrystalline yttrium iron garnet (YIG), for example, is at least several times larger than single-crystal linewidths, and it is also found to depend on the microstructure of the material.[4] In addition, HFE linewidth data for polycrystalline ferrites generally show a pronounced tail that extends very far out in the field above the manifold region. Secondary two-magnon scattering effects[23,24] are too weak to explain this tail response.

This paper presents high-accuracy data and analyses for the HFE linewidth in polycrystalline YIG materials that resolve many of these problems. The data show that the above manifold tail for the HFE linewidth in dense YIG spheres correlates with the density of states for low wave number electromagnetic-spin-wave (EMSW)[25] modes. Past effective linewidth analyses and loss models have, in general, ignored these modes. It is found, moreover, that a proper extrapolation of the HFE linewidth to very high fields gives ΔH_{eff} values that match intrinsic linewidths in single-crystal YIG.

II. HIGH-FIELD EFFECTIVE LINEWIDTH TECHNIQUE

Following the introduction of this parameter by Kohane and Schlömann,[1] the HFE linewidth simply expresses the relaxation rate η of the driven mode in field units through the connection $\Delta H_{\text{eff}}(H) = 2\eta(H)/|\gamma|$, where H is the static external field and γ denotes the gyromagnetic ratio of the ferrite. It is the relaxation rate that is field dependent, while ΔH_{eff} just gives this parameter in recognizable units. Typical FMR linewidths in single-crystal ferrites are in the order of 1 Oe.

[a]Electronic mail: monan@lamar.colostate.edu

 © 2005 American Institute of Physics

Downloaded 07 Jul 2005 to 129.82.31.230. Redistribution subject to AIP license or copyright, see http://jap.aip.org/jap/copyright.jsp

While polycrystalline materials usually have linewidths from tens to hundreds of Oersteds. As noted above, the high-field ΔH_{eff} can be much smaller than the FMR linewidth.

The effective linewidth measurement technique is discussed by Truedson *et al.*[10] and the references cited therein. The $\Delta H_{\text{eff}}(H)$ determinations are made through high-precision measurements of the cavity center frequency f and quality factor Q as a function of H. Typically, the measurements utilize a high- Q cavity with a ferrite sample installed inside and standard scalar analyzer microwave techniques. The change in f and Q with field can be related to ΔH_{eff} through the cavity perturbation theory and the dynamic magnetization response equations, with loss terms included.

The working formulas for the field dependences of f and Q for a spherical isotropic ferrite sample at high field may be written as

$$f = -\frac{1}{K}X_f + f_\infty \tag{1}$$

and

$$\frac{1}{Q} = \frac{\Delta H_{\text{eff}}}{K}X_Q + \frac{1}{Q_\infty}. \tag{2}$$

The f and f_∞ denote frequencies in hertz. The parameters X_f and X_Q are functions of field according to

$$X_f = \frac{4\pi M_s H f}{H^2 - (2\pi f/|\gamma|)^2} \tag{3}$$

and

$$X_Q = \frac{4\pi M_s[H^2 + (2\pi f/|\gamma|)^2]}{[H^2 - (2\pi f/|\gamma|)^2]^2}. \tag{4}$$

In the extreme high field limit, X_f and X_Q tend to zero as $1/H$ and $1/H^2$, respectively. The f_∞ and Q_∞ correspond, therefore, to the f and Q of the cavity with the magnetic effects frozen out, so to speak. The K parameter is a cavity calibration factor and $4\pi M_s$ denotes the saturation induction of the sample. The above formulas are valid in the high-field limit in which the condition $H \gg \Delta H_{\text{eff}}$ is satisfied. All equations here and below are in Gaussian cgs units.

The determination of $\Delta H_{\text{eff}}(H)$ is done in two steps. One first measures f as a function of H, plots f as a function of the X_f parameter, and obtains the calibration factor K from fits of the data to Eqs. (1) and (3). In the high-field regime, such plots are generally quite linear, and the K value is reasonably close to values from standard cavity perturbation theory.[10]

The optimum linear fit of the data to Eqs. (1) and (3) in step 1 also requires an accurate value of the gyromagnetic ratio γ. If γ is not set appropriately, this fit will be poor. In this work, the value of γ was adjusted to optimize the linearity of the measured f versus X_f response. This γ-determination procedure resolves several problems in previous in-manifold and high-field effective linewidth work.[9] In those works, the free-electron value of 2.8 MHz/Oe for $|\gamma|/2\pi$ was taken to be correct in the high-field limit only, and $\gamma(H)$, along with $\eta(H)$, were then determined as a function of field from the $f(H)$ and $Q(H)$ data and the cavity perturbation theory. This approach led to notable anomalous field dependences for both γ and ΔH_{eff}.

In the second step, one takes the $Q(H)$ data, applies Eqs. (2) and (4), and obtains $\Delta H_{\text{eff}}(H)$. In practice, $f(H)$ and $Q(H)$ are measured simultaneously. In addition, the field is stepped back and forth between the lowest-measurement field (field A) and a high-field reference point (field B) in small increments. The full set of data points for a given field value are then correlated against the field A data points and analyzed to minimize drift effects and improve accuracy. This measurement sequence, called the "modified ABA technique" in metrology language, is further elaborated below.

It is to be emphasized that accuracy is paramount for a meaningful HFE linewidth measurement. The experiment is performed on the extreme high-field tail of the FMR absorption line, at fields that are 1 kOe or more above the FMR field. With actual FMR linewidths in the 15–30-Oe range, this means that one is measuring the loss component of the susceptibility at fields from several tens to several hundreds of linewidths away from the FMR peak. Under these conditions, the HFE linewidths are derived from extremely small changes in the cavity frequency f and Q with field.

Accuracy was optimized through the use of a high- Q cavity and the systematic ABA measurement procedure indicated above to minimize the effect of random errors and drifts. For a given set of $f(H)$ and $Q(H)$ measurements, data were obtained by cycling the field from the measurement field H-point to some high-field reference point and back again many times. From the average of the f and Q values data for a given field, and the change from the high-field reference, random errors and drift effects are largely eliminated. Through simultaneous measurements of the cavity temperature through this sequence, one also obtains a determination of the average change in f and Q with temperature, so that these thermal changes can be compensated as well.

III. MATERIALS AND MEASUREMENT DETAILS

The measurements were made on two types of YIG materials, near theoretical density YIG samples produced by hot isostatic pressing[15] and conventionally sintered (CS) commercial G113 samples produced by Trans Tech. The hot isostatic pressed (hipped) and the CS samples had densities greater than 99.9% and 99.0%, respectively, relative to the theoretical YIG density. The measurements were made on nominal 2-mm-diameter polished spheres at a nominal frequency of 10 GHz. The high density leads to a small FMR linewidth. The 9.5-GHz half power FMR linewidths for the hipped and the CS samples were 13.5 and 30 Oe, respectively. The nominal saturation induction of these YIG materials was taken as 1750 G. The fitted $|\gamma|/2\pi$ values for the hipped and CS samples were obtained as 2.76 and 2.74 MHz/Oe, respectively.

Measurements were made with a high- Q cylindrical TE_{011} transmission cavity fabricated from oxygen-free high-conductivity copper, with the sample positioned at the cavity center. The nominal center frequency and Q factor of the cavity were 10 GHz and 22 000, respectively. A modified

Downloaded 07 Jul 2005 to 129.82.31.230. Redistribution subject to AIP license or copyright, see http://jap.aip.org/jap/copyright.jsp

ABA measurement procedure made it possible to reduce the uncertainty in the high-field Q determinations ten fold, relative to previous work, as in Ref. 6, for example. The error in Q was typically in the ±1 to ±3 range. The empty cavity response was checked over a range of H values from 1 to 9.5 kOe. The empty cavity center frequency remained constant to within a few tenths of kHz. Such small changes are negligible in comparison to the frequency shift due to the sample. The empty cavity Q factor did show a small change with field on the order of about 0.5 per kOe. These changes were not considered to be significant relative to the measurement errors.

For YIG spheres at 10 GHz, the manifold region of degenerate moderate- k spin waves extends over a range of H values of about 3.38 to 4.15 kOe. The HFE linewidth measurements were made for H values from 4.5 to 8 kOe or so. The lower limit is well above the manifold upper limit field. The separation from the upper manifold limit of 300–400 Oe was chosen to avoid primary and secondary two-magnon scattering effects.[23,24] The upper limit is still low enough to allow for a reasonable accuracy for the Q measurements. The high-field limit is somewhat lower than the 10–12 kOe values used in some previous HFE linewidth studies. For such very high fields, the accuracy of the measurement is extremely low. As the new data show, such high fields are not needed to obtain good linewidth extrapolations to intrinsic values in the high-field limit.

IV. HIGH-FIELD EFFECTIVE LINEWIDTH RESULTS

Figure 1 provides a view of the step-by-step analysis of the $f(H)$ and $Q(H)$ data that yield $\Delta H_{\text{eff}}(H)$. The open circle data in all three graphs are for the hipped YIG sphere. The open square data in Fig. 1(c) are for the CS sample. Figure 1(a) shows the data on the frequency versus field displayed in a $f(X_f)$ format that shows the linear dependence discussed in Sec. II. As already noted, the γ values for the samples were adjusted to optimize the linearity of the f versus X_f response. The accuracy of the f data in Fig. 1(a) is about ±0.5 kHz. The solid line shows the linear fit. Figure 1(b) shows the companion plot of the Q versus field data shown in a $Q^{-1}(X_Q)$ format. The accuracy of the Q data in Fig. 1(b) is about ±1.5. The solid curve in Fig. 1(b) is a quadratic fit to the data. Figure 1(c) then shows the values of the HFE linewidth as a function of X_Q, as obtained from Fig. 1(a) and 1(b). Figure 1(c) also shows a solid linear line fit to the hipped YIG data and a dashed line fit to the CS sample data for X_Q values below about 4.5×10^{-5} Oe^{-1}. The accuracy of the ΔH_{eff} points in Fig. 1(c) is in the 0.01–0.2 range, depending on the field.

Figure 1(a) shows that the cavity frequency is indeed a linear function of the X_f inverse-field parameter, as expected from perturbation theory and the dispersion component of the microwave susceptibility response analysis that leads to the $X_f(H)$ functional form in Eq. (3). The calibration parameter K, as obtained from the slope of the response in Fig. 1(a), is also in accord with microwave perturbation theory. The numerical value of K from the linear fit in Fig. 1(a) is 1746. The perturbation theory value for K is 2207. This

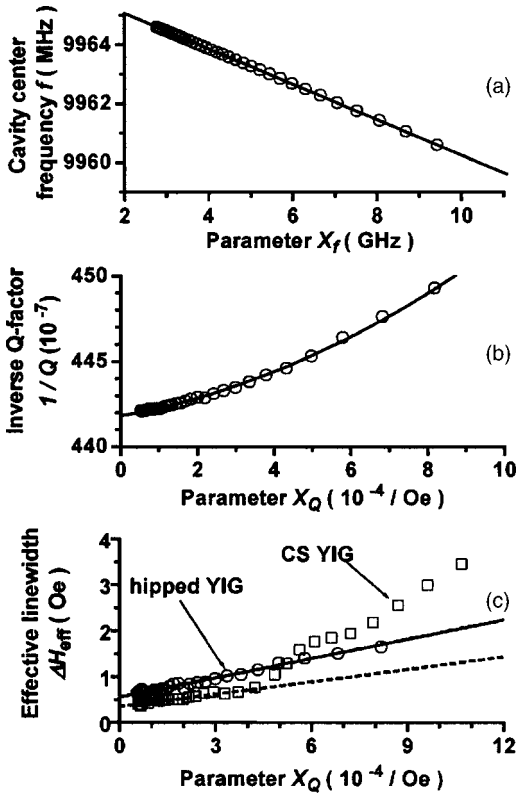

FIG. 1. The open circle data points in graphs (a) and (b) show the cavity frequency f and inverse Q as a function of the parameters X_f and X_Q, respectively, for the hipped YIG sample. Graph (c) shows the high-field effective linewidth ΔH_{eff} as a function of X_Q. The open circles and squares show the hipped and CS YIG results, respectively. The solid lines in (a) and (c) show linear fits to the open circle points. The solid line in (b) show a quadratic fit to the data. The dashed line in (c) shows a linear fit to the solid circle points for low X_Q values below about 4.5×10^{-4} Oe^{-1}.

change is due to the small distortions in the empty cavity mode that result from the nonzero sample volume.[10] In Ref. 10, Truedson *et al.* show that in the limit of a vanishingly small sample volume, the empirical K value approaches the perturbation theory prediction. One of the important advantages of the empirical calibration is the more accurate K value and the corresponding improved value for $\Delta H_{\text{eff}}(H)$.

Figure 1(a) and the numerical slope value obtained therefrom show that perturbation theory is applicable in form and that the empirical calibration parameter K can be trusted. This is supported by the previous work by Truedson *et al.*,[10] on the effect of sample size on K and the convergence to the perturbation theory value in the limit of very small samples.

Figures 1(b) and 1(c) shows the rather astounding high-field ΔH_{eff} result relative to previous data. At first glance, Eq. (2) suggests that $1/Q$ as a function of X_Q should show a linear response with a slope of $\Delta H_{\text{eff}}/K$. Figure 1(b), however, shows that $1/Q$ versus X_Q *is actually quadratic*. This means that the effective linewidth actually *decreases* as the field is increased. Recall from Eq. (4) that lower values of X_Q mean higher values of the field H. From Eq. (2), it is evident that the hipped YIG data in Fig. 1(c) correspond essentially to the slope of the response in Fig. 1(b). The graph actually shows this slope multiplied by the calibration factor K, and this corresponds to ΔH_{eff}. It can also be seen that the hipped YIG material shows a linear ΔH_{eff} versus X_Q, while the CS

Downloaded 07 Jul 2005 to 129.82.31.230. Redistribution subject to AIP license or copyright, see http://jap.aip.org/jap/copyright.jsp

sample has an HFE linewidth that is linear only for lower X_Q or relatively high fields. For the CS sample, ΔH_{eff} appears to rise rapidly at high X_Q and corresponding fields.

The results in Figs. 1(b) and 1(c) run counter to almost all of the previous results on the high-field effective linewidth in polycrystalline ferrite materials. In many of these works, the high-field ΔH_{eff} obtained far outside the manifold region was taken to be constant, based on the idea that there were no degenerate spin waves at the signal frequency for high fields. The accuracy in ΔH_{eff} for the data in those works was about $\pm 1 - \pm 2$ Oe, and it was not possible to discern any clear change in ΔH_{eff} with field in the high-field regime.

The high-accuracy results shown here indicate that this old picture is in need of major revision. There are three points of note. First, the hipped YIG shows a linear ΔH_{eff} versus X_Q response. As Sec. V will show, this translates into a decrease in the HFE linewidth, with an increasing field that closely matches the density of states for degenerate electromagnetic branch spin waves. This new connection is one of the key results of this work. Previously, the role of the electromagnetic spin waves and the two-magnon scattering in the high-field effective linewidth was completely ignored. It is also clear from the different responses for the hipped and CS samples that the field response is affected by microstructure. These connections will be discussed in Sec. V.

Second, the data show that the extrapolated ΔH_{eff} in the high-field $X_Q \rightarrow 0$ limit is very close to the known intrinsic linewidths in single-crystal YIG. At 10 GHz, such linewidths lie typically in the 0.5-Oe range. The present data represent the first measurement of a near-intrinsic high-field effective linewidth in a polycrystalline ferrite. The combination of a previously unrealized field dependence and the experimental demonstration of an intrinsic linewidth in the high-field limit also shows that the HFE linewidth concept proposed by Kohane and Schlömann (KS)[1] is correct. The high-field limit does indeed give ΔH_{eff} values that are close to single-crystal intrinsic values that are not affected by the microstructure. The only caveat to the KS concept is in the previously unrealized role of high-field two-magnon scattering that involves the electromagnetic spin wave (EMSW) branches of the dispersion. This connection is developed below.

Third, the clear differences in the high-field $\Delta H_{\text{eff}}(X_Q)$ responses for the hipped and CS samples mark the effect of porosity on the effective linewidth for fields close to the manifold region. It was noted above that the CS data show a linear response with a near-intrinsic $X_Q \rightarrow 0$ extrapolation only for X_Q values below about 4.5×10^{-5} Oe^{-1}. There is an apparent break at $X_Q \approx 4.5 \times 10^{-5}$ Oe^{-1}, with a more rapid rise in ΔH_{eff} as X_Q is further increased. Hoeppe has recently published a detailed analysis of the effective linewidth in porous ferrites.[17] He has proposed that the dipole field around the pores can cause an artificial shift in the upper field limit for the manifold region to higher values of the static field. His data and analyses support his proposal. The results indicate that for YIG materials, this shifted manifold limit field is just at the corresponding X_Q break point apparent in Fig. 1(c). The high-accuracy data shown in Fig. 1 corroborate and extend this model. Not only do the data show the break point and the quasimanifold two-magnon scattering to low wave number spin-wave modes for lower fields and high X_Q. The results also show that for low X_Q, there is a clear transition to a different mode of scattering that yields a near-intrinsic linewidth in the high-field $X_Q \rightarrow 0$ limit.

V. DIPOLE EXCHANGE AND ELECTROMAGNETIC SPIN-WAVE BANDS AND EFFECTIVE LINEWIDTH CONNECTIONS

By way of introduction, it is useful first to consider the standard moderate- k spin-wave dipole-exchange spin-wave (DE-SW) band described through the well-known dispersion equation[22]

$$\omega_k(k,\theta_k) = |\gamma| \sqrt{(H_i + Dk^2)(H_i + Dk^2 + 4\pi M_s \sin^2 \theta_k)}, \quad (5)$$

where ω_k is the spin-wave angular frequency, θ_k is the angle between the wave vector $\mathbf{k}$ and the static internal field, H_i denotes the value of the static internal field, and D is an exchange stiffness parameter. This relation is valid under two conditions. First, the spin-wave wavelength $\lambda_k = 2\pi/k$ must be much smaller than the dimensions of the sample so that surface dipole fields can be neglected. Second, k must be much larger than the corresponding pure electromagnetic wave number $k_{\text{emk}} = \sqrt{\varepsilon_r}\omega_k/c$, where ε_r is the relative dielectric constant of the material and c is the speed of light in vacuum. The $k \gg k_{\text{emk}}$ condition ensures that displacement currents and electromagnetic propagation effects can be neglected. This second condition may also be written as $\omega_k \ll \omega_{\text{emk}}$. In other words, $\omega_k(k,\theta_k)$ is far from the light line defined by $\omega_{\text{emk}} = ck/\sqrt{\varepsilon_r}$. This limit is often called the "magnetostatic approximation" and the band is called the "magnetostatic spin-wave band." For purposes of this discussion, the wave number k is always taken as positive and real.

Figure 2 shows this DE-SW spin-wave band. The plot shows the spin-wave frequency $\omega_k/2\pi$ in GHz as a function of k in rad/cm. The band limits are for limit θ_k values of 0° and 90° as indicated. The contours indicate the continuum nature of the band for large samples. The specific diagram shown here was computed for $|\gamma|/2\pi = 2.8$ GHz/kOe, an H value of 4.5 kOe, $D = 5.2 \times 10^{-9}$ Oe cm^2, and $4\pi M_s = 1750$ G. For a sphere, the corresponding internal field is obtained as $H_i = H - (4\pi M_s/3)$. The $H = 4.5$ kOe point is chosen to be close to the kink point in Fig. 1(c) at $X_Q = 4.5 \times 10^{-5}$ Oe^{-1}. There are also two points of reference in the diagram, the light line at ω_{emk}, obtained for $\varepsilon_r = 10$, and a dashed horizontal line at the nominal operating frequency of 10 GHz.

The curvature of the band contours is due to exchange. The minimum frequency point at $\omega_k(0,0°) = \omega_H = |\gamma| H_i$ is due to the Zeeman energy. The band is formed because of the dipole-dipole energy associated with wave vectors that are not parallel to the vector field $\mathbf{H}$. The top band limit frequency for $k = 0$ is given by $\omega_k(0,90°) = \omega_B = |\gamma| \sqrt{H_i(H_i + 4\pi M_s)}$. Both points are indicated on the vertical axis in Fig. 2.

It is important to note the position of the band in Fig. 2 relative to the 10-GHz operating point, and observe that there are no spin-wave modes that are degenerate with this

Downloaded 07 Jul 2005 to 129.82.31.230. Redistribution subject to AIP license or copyright, see http://jap.aip.org/jap/copyright.jsp

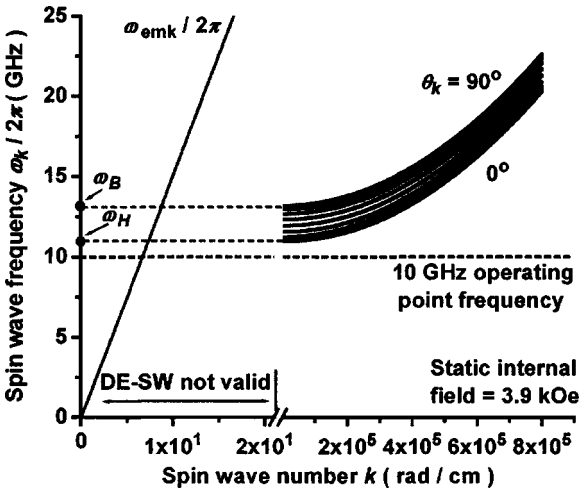

FIG. 2. The dipole-exchange spin-wave (DE-SW) band in the magnetostatic limit. The graph shows the spin-wave frequency $\omega_k/2\pi$ as a function of the positive real wave number k for YIG parameters, an external field of 4.5 kOe (or an internal field of 3.9 kOe, as indicated), and sphere-demagnetizing factors. The band of contours corresponds to propagation angles θ_k, relative to the static internal field, that range from 0° to 90°, as indicated. The band was evaluated from Eq. (5) with parameters as listed. The graph also shows the electromagnetic wave dispersion given by ω_{emk}, with the relative dielectric constant equal to 10, and a reference line at the signal frequency of 10 GHz. The low- k limit frequencies of the DE-SW spin-wave band, ω_H and ω_B, are indicated on the vertical axis. The horizontal dashed lines extended from the band to these frequency points are intended to emphasize that the DE-SW dispersion is not applicable in this low-k regime.

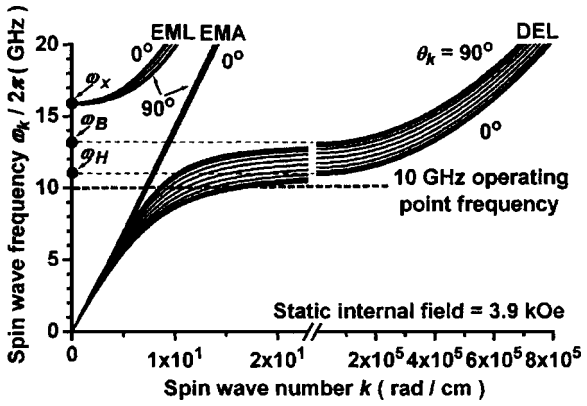

FIG. 3. Diagram of the three full spin-wave bands for an infinite medium. The graph shows the curves for the spin-wave frequency $\omega_k/2\pi$ as a function of the positive real wave number k for YIG parameters at a static internal field of 3.9 kOe. The bands of contours correspond to propagation angles θ_k, relative to the static field, that range from 0° to 90°, as indicated. These curves group into three bands, the dipole-exchange Larmor (DEL) band, the electromagnetic Larmor (EML) band, and the electromagnetic anti-Larmor (EMA) band, as indicated. The bands were evaluated from Eq. (6) and for the same parameters as used for Fig. 2. The graph also shows a reference line at the signal frequency of 10 GHz. The moderate- k band limit frequencies, ω_H and ω_B, from Fig. 2 and the new EML limit frequency at $k=0$, ω_X, are also indicated.

signal frequency. Note further that the band shifts with field. If H is increased, the band will shift to even higher frequencies and the band of DE-SW excitations will move even farther away from the signal frequency. Based on this picture, excitations within the spin-wave band should, therefore, have no effect on the losses for the driven uniform mode at the signal frequency for any field such that the condition $\omega_H > \omega$ is satisfied. This absence of degenerate modes at the signal frequency was, in the past, the basis of the argument that the high-field effective linewidth should (1) not involve two-magnon scattering, (2) be field independent, and (3) be equal or close to the intrinsic linewidth of the ferrite.

The much more complicated spin-wave band that results from a full solution of Maxwell's equations and the linearized torque equation of motion for plane spin waves tells a different story. The governing equation for these excitations can be written in the form

$$H_i = 4\pi M_s\left[\frac{k^2(1+\cos^2\theta_k)}{2(k^2-k_{\mathrm{emk}}^2)}-1\right] - Dk^2 \pm \sqrt{\frac{\omega_k^2}{|\gamma|^2}+\frac{(4\pi M_s)^2k^4\sin^4\theta_k}{4(k^2-k_{\mathrm{emk}}^2)^2}} = H-\frac{4\pi M_s}{3}. \tag{6}$$

All parameters are the same as given previously. Except for the last $H-(4\pi M_s/3)$ connection to make the result specific to spherical samples, Eq. (6) is completely general.

It is clear from the form of Eq. (6) that a rearrangement of terms will lead to a quartic equation in k^2 and four pairs of roots. It turns out that there are three real root pairs and one imaginary root pair if the frequency ω_k is greater than $\omega_X = |\gamma|(H_i+4\pi M_s)$. There are two real and two imaginary root pairs for $\omega_k < \omega_X$. It will prove convenient to denote the root pairs as $\pm k_{\mathrm{DEL}}$, $\pm k_{\mathrm{EML}}$, $\pm k_{\mathrm{DEA}}$, and $\pm k_{\mathrm{EMA}}$, where DE stands for dipole-exchange spin waves, EM stands for electromagnetic spin waves, L stands for Larmor precession, and A stands for anti-Larmor precession. The reason for these labels will become clear shortly. As one scans θ_k from 0° to 90°, each of these solutions will create a band of allowed excitations, just as the dispersion in Eq. (5) creates the band shown in Fig. 2.

Figure 3 shows the frequency $\omega_k/2\pi$ in GHz as a function of k in rad/cm, for the bands calculated from the real positive k roots of Eq. (6). The parameters and field conditions are the same as for Fig. 2. Now, however, there are three bands that correspond to the just labeled dipole-exchange Larmor (DEL) spin waves, electromagnetic Larmor (EML), and electromagnetic anti-Larmor (EMA) excitations, as indicated. As before, the band interior contours indicate the continuum nature of the band for large samples. As in Fig. 2, a reference line at $\omega_k/2\pi=10$ GHz is shown. The manifold limit frequencies ω_H and ω_B from Fig. 2 and the new frequency parameter ω_X are indicated along the vertical axis.

It is useful to note several connections between Fig. 3 and the DE-SW picture in Fig. 2. First, for moderate to large k values, the DEL spin waves correspond closely to the DE-SW spin-wave band in Fig. 2. The nearly horizontal DEL band limit lines for 10^2 rad/cm $< k < 10^4$ rad/cm or so correspond to the DE-SW low- k band edges at ω_B and ω_H. In addition, the nearly straight EMA dispersion and the extremely narrow band correspond closely to the light line in Fig. 2 described by $\omega_{\mathrm{emk}}=ck/\sqrt{\varepsilon_r}$. The only band not shown in Fig. 2 in some form is the EML band. This band starts at the ω_X point that is somewhat above ω_B, and then merges

Downloaded 07 Jul 2005 to 129.82.31.230. Redistribution subject to AIP license or copyright, see http://jap.aip.org/jap/copyright.jsp

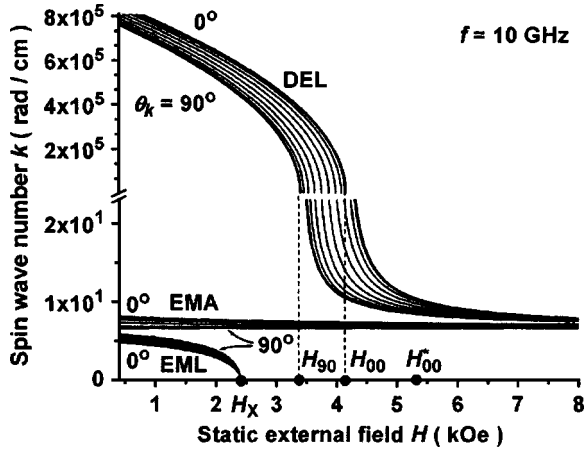

FIG. 4. Diagram of the three spin-wave bands in a wave number vs field format for fixed frequency. The graph shows the curves for the spin-wave wave number k as a function of the static external field H at a fixed frequency f of 10 GHz for the full range of propagation angle θ_k from 0° to 90°, as indicated. As in Fig. 3, the curves group into three bands, the dipole-exchange Larmor (DEL) band, the electromagnetic Larmor (EML) band, and the electromagnetic anti-Larmor (EMA) band, as indicated. The bands were evaluated from Eq. (6) and for the same parameters as used for Figs. 2 and 3. The graph shows four important field points along the H axis, an H_X field that corresponds to the ω_X frequency point in Fig. 3, the moderate- k band limits in the field at $H=H_{90}$ and $H=H_{00}$ that correspond to the frequency limits ω_B and ω_H in Figs. 2 and 3, and an additional field point shifted up from H_{00} by $8\pi M_s/3$, and denoted as H_{00}^*.

with the DEL light line branch at high frequency. It is important to emphasize that these bands are not new. They are discussed in Ref. 25. Their detailed characteristics have also been discussed in Ref. 26 for cases in which loss and conductivity effects are included.

For the ensuing discussion, it will prove convenient to cast the $\omega_k(k,\theta_k)$ band picture in Fig. 3 for a constant static field into a band picture in which k is given as a function of the external field H and the angle θ_k for a fixed ω_k value equal to the signal frequency ω. Figure 4 shows such a presentation for $\omega_k/2\pi=10$ GHz. No curves or bands are shown for $H<4\pi M_s/3$ because this would correspond to negative internal fields.

In this new format, the manifold region now corresponds to the vertical section of the DEL band for $H_{90}=3.38$ kOe $<H<H_{00}=4.15$ kOe. The k versus H format in Fig. 4 is particularly useful here because one can see immediately the range of modes that are degenerate with the signal frequency. If one were considering DE-SW excitations only, there would be *only one band*, the DEL band, and *even this band would truncate below* $k=300$ rad/cm or so. In that case, there would be no spin-wave excitations available at the signal frequency for fields above the upper limit manifold band edge at H_{00}. If the dipole fields from spherical pores are taken into account, this cutoff band edge is shifted up in field by $8\pi M_s/3$ to H_{00}^*.[17]

However, when the full band picture in Fig. 4 is considered, one can see that there are always *some* spin-wave modes that are degenerate with the signal frequency. The high-frequency transition frequency ω_X in Fig. 3 now converts to a transition field H_X, as indicated. For any field $H>H_X$, there will always be two real and positive root solutions to Eq. (3) for a given θ_k. For $H<H_X$, there will be three roots. The corresponding root solutions for the full range of θ_k from 0° to 90° give rise to the indicated bands.

One can also see from Fig. 4 that the two surviving bands for $H>H_X$ become extremely narrow in the limit of very high fields. Two-magnon scattering processes that involve excitations in these two-tail bands is proposed as the source of the experimental effective linewidth responses presented above. The field dependence of ΔH_{eff} in Sec. IV is attributed to the shrinkage in the field width of these bands at $\omega_k=\omega$ with increasing field. The near-intrinsic effective linewidth in the high-field limit is attributed to this shrinkage to zero width and band convergence to the light line.

VI. TWO-MAGNON SCATTERING AND THE HIGH-FIELD EFFECTIVE LINEWIDTH

Two-magnon scattering from the uniform mode to degenerate spin waves is a well established relaxation process for ferromagnetic resonance. Quantitative connections have been made to the FMR linewidth in single-crystal and polycrystalline ferrites[21,27] as well as the near-FMR effective linewidth for fields within the manifold region. It is well established that the source of the scattering in these cases consists of various inhomogeneities such as surface pits, porosity, and the magnetocrystalline anisotropy in the randomly oriented grains in polycrystals.[22,28]

Two-magnon relaxation in the context of FMR in ferrite materials is reviewed by Sparks.[22] Simply stated, inhomogeneities related to pores, grains, or pits of some size a in the micron range couple the uniform mode to degenerate spin waves with wave numbers in the range from zero to about π/a. For typical polycrystalline ferrite with a values in the range of $1-10$ μm, this means that only the degenerate modes with k values below about 10^3-10^4 rad/cm can contribute to the scattering. From the traditional spin-wave band picture in Fig. 2, such modes would be only available for scattering for fields below the upper field manifold region cutoff point H_{00} shown in Fig. 4.

The new data presented above, and the situation depicted in Fig. 4, provide a strong motivation to reexamine these old assumptions. It is important to note that any high-field two-magnon process must involve extremely low k modes. From Fig. 4, one can see that the degenerate modes for fields above $4-5$ kOe or so have k values below $100-150$ rad/cm and drop even lower at higher fields. One important question concerns the efficiency with which micron and submicron sized inhomogeneities can produce scattering to such low- k modes with wavelengths of a few tenths of a millimeter or larger.

An important test of a possible two-magnon term in the HFE linewidth would be to make a quantitative comparison between the field dependence of the density of states (DOS) for the $\omega_k=\omega$ spin waves in the degenerate modes in the DEL and EMA bands in Figs. 3 and 4 with the field dependence of the HFE linewidth. Density of states is a basic concept in solid-state physics. The starting assumption is that the allowed plan-wave modes are uniformly distributed in **k** space. It is then a matter of geometry and the details of the given dispersion connections to obtain the number of modes

Downloaded 07 Jul 2005 to 129.82.31.230. Redistribution subject to AIP license or copyright, see http://jap.aip.org/jap/copyright.jsp

$dn(\omega_k)$ for a given slice of frequency space from ω_k to $\omega_k + d\omega_k$. The relation $dn(\omega_k) = g(\omega_k)d\omega_k$ then serves as a definition of a DOS function $g(\omega_k)$.

For the multiband spin-wave situation at hand, $g(\omega_k)$ goes over to a field-dependent $\tilde{g}(\omega_k, H)$ DOS function. This is because the k solutions in Eq. (6) also depend on H. One obtains a working equation of the form

$$\tilde{g}(\omega_k, H) = \frac{1}{\pi}\sum_b \left[\int_0^{\pi/2} k^2 - (\omega_k, \theta_k, H)\frac{\partial k(\omega_k, \theta_k, H)}{\partial \omega_k} \sin\,\theta_k d\theta_k \right]_b . \quad (7)$$

The sum parameter b refers to the available bands. For the HFE linewidth situation, there are two bands, the DEL and the EMA bands, as in Fig. 4. For the two-magnon scattering problem, one solves Eq. (6) for the two positive real $k(\omega_k, \theta_k, H)$ roots for the DEL and EMA bands, obtains the derivative functions needed for Eq. (7), and then evaluates the integrals for $\omega_k = \omega$. These evaluations are done numerically to obtain $\tilde{g}(\omega, H)$ as a function of H.

Figure 5 shows plots of the combined two-band density of states (DOS) at the signal frequency ω as a function of the static external field H in the high-field regime, along with suitably scaled plots of the measured high-field ΔH_{eff} versus H. Figures 5(a) and 5(b) show separate comparisons for the hipped and CS YIG samples, respectively. Note that the common left-most field limit for the graphs is well above the upper manifold band-edge field H_{00} value of 4.15 kOe. The upshifted H_{00}^* point at $H_{00} + 8\pi M_s/3$ from Fig. 4 is indicated on the field axes for both graphs. The vertical axes have been scaled and shifted in both cases to yield approximate qualitative matches with the DOS curves for $H > H_{00}^*$. The error bars on the data points indicate the uncertainty of the ΔH_{eff} values from the modified ABA measurements. For use in the discussion below, the label H_{00}^* indicate the highest field point to which the local upper manifold band edge would be shifted due to dipole fields around a pore in a YIG sphere.

The results in Fig. 5 show three things. First, both graphs show that the HFE linewidth tracks the DOS response reasonably well for fields above the H_{00}^* point. Second, the data indicate high-field limit values for ΔH_{eff} in the 0.5–0.6 Oe intrinsic linewidth range. This is in line with the results from the ΔH_{eff} versus X_Q extrapolations in Fig. 1(c). Third, for fields below H_{00}^*, the ΔH_{eff} data for the CS sample in Fig. 5(b) show a distinct departure from the DOS curve. One can see that (1) the departure in the HFE linewidth values from the DOS response is rather abrupt and (2) this jump occurs very close to the $H = H_{00}^*$ marker. These departures from the DOS line are relatively large, in the 0.5–2-Oe range.

These results indicate that there are *two distinct two-magnon scattering contributions to the HFE linewidth*. Both of them are turned off in the extreme high-field limit because of the shrinking spin-wave bands and their convergence with the light line. In this limit, one obtains an extremely low linewidth that matches closely with known intrinsic single-crystal linewidths. This conclusion applies to both the hipped YIG and the CS samples. This long sought after and previously unrealized result is extremely satisfying.

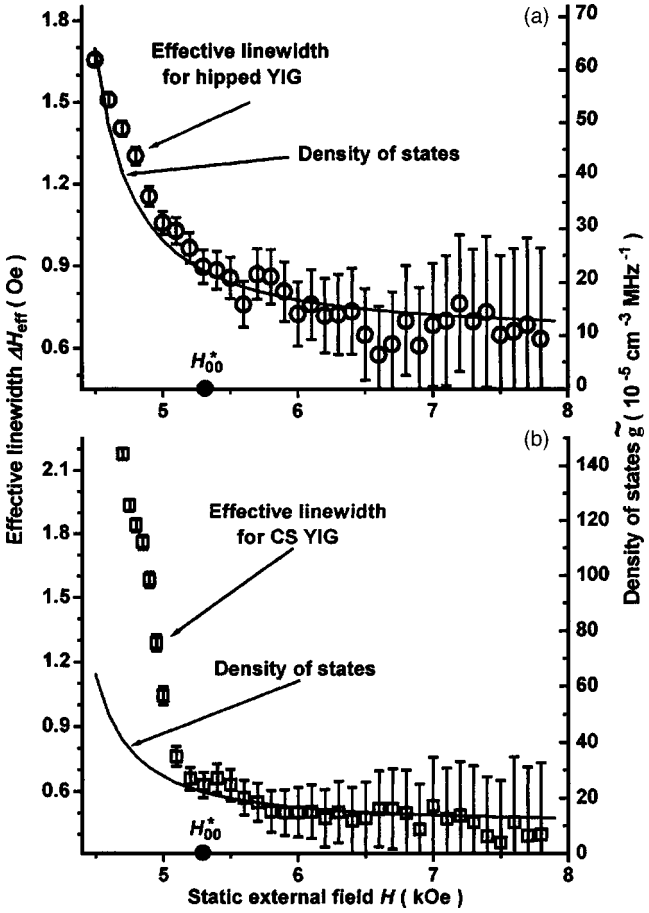

FIG. 5. Graphs of the high-field effective linewidth ΔH_{eff} and the total electromagnetic spin-wave two-band density of states $\tilde{g}$ as a function of the static external field. The open circles in graphs (a) and (b) and the corresponding error bars show the measured effective linewidth data for the hipped and CS YIG samples, respectively. The solid curves show the calculated density of states for degenerate electromagnetic spin-wave modes at the signal frequency, as a function of the field. The H_{00}^* point indicates the effective band-edge field when the dipole field of spherical pores is accounted for.

As the field is first reduced, one sees the growing contribution of low- k electromagnetic spin-wave scattering to the ΔH_{eff}. This is evidenced by the gradual rise in the HFE linewidth for fields down to the H_{00}^* field point. This rise, moreover, scales nicely with the computed density of states for these modes. There are no adjustable parameters in the DOS calculation. In Fig. 1(c), the slope of the ΔH_{eff} versus X_Q response is slightly larger for the CS than for the hipped YIG. This implies that the scattering to the low- k EM-SW modes is stronger for the less dense microstructure. The fundamental details of this scattering process need further work.

Finally, for fields below H_{00}^*, the abrupt rise in ΔH_{eff} above the DOS response for the CS sample signals the onset of manifold scattering to moderate- k spin-wave modes within the conventional DE-SW band. Following the arguments of Hoeppe, this onset point is shifted up from the expected onset field point at H_{00} because of the dipole fields around residual pores and other possible inclusions. Here, too, the value of the onset field H_{00}^* is based solely on the working equations for the spin-wave band and known dipole field considerations. There are no adjustable parameters.

Downloaded 07 Jul 2005 to 129.82.31.230. Redistribution subject to AIP license or copyright, see http://jap.aip.org/jap/copyright.jsp

VII. FURTHER COMMENTS ON TWO-MAGNON SCATTERING

As outlined in Sec. I and at the beginning of Sec. VI, two-magnon scattering has been well established over a span of over four decades as the dominant FMR loss mechanism in weakly inhomogeneous magnetic systems. The new results presented herein demonstrate a rather unexpected and previously unexamined corollary—that extremely low k two-magnon scattering also plays a critical role in the high-field off-resonance losses.

There is a strong connection between these results on the two-magnon HFE linewidth in ferrites and the various two-magnon mechanisms for thin films that have come into focus recently. As with the ferrite work, theoretical and experimental studies of two-magnon scattering in magnetic films extends back to the 1960s. While the renewed interest is driven, in part, by possible microwave applications, it is predominantly driven by ultrathin metallic film applications in high-density, high-speed magnetic recording.

Two-magnon scattering in thin films was first applied by Wigen[29] to spin-wave resonance linewidth data for perpendicularly magnetized thin Permalloy films with pinned surface spins. In 1967, Patton *et al.*,[30] proposed two-magnon processes to explain FMR linewidth data as a function of frequency and film thickness for in-plane magnetized films. Sparks[31] and Hurben and Patton[32] further applied two-magnon concepts to single-crystal ferrite films. The key advances that have triggered the modern reexamination of two-magnon scattering in thin films are in the often-cited work by Arias and Mills[33] in which a short-wavelength variation in the thickness-dependent surface anisotropy field provides a mechanism for scattering. In thin films, and especially in ultrathin films, the spin-wave dispersion is severely modified from the bulk relations given above.[34] There has been further theoretical work by McMichael and Krivosik[18] and Dobin and Victora,[20] as well as data by Azevedo *et al.*,[12] McMichael and Krivosik,[18] Cochran *et al.*,[35] and Heinrich and Cochran.[36]

It is important to note, however, that there have been only a few attempts to measure off-resonance effective linewidths in thin films, and these have met with only modest success. The near-resonance effective linewidths in Permalloy films was studied by Patton *et al.*[5] and Moosmüller *et al.*[8] Kabos and Patton[37] examined the effective linewidth in YIG films. With the possibility of high-precision cavity measurements as demonstrated above, there are possibilities to apply the HFE linewidth approach to two-magnon and intrinsic processes in thin films.

VIII. SUMMARY AND CONCLUSION

The above sections have described a refined technique for the precision measurement of the high-field effective linewidth in bulk ferrite materials. Specific measurements are reported for two materials, ultradense polycrystalline yttrium iron garnet produced by hot isostatic pressing and conventional sintered (CS) YIG with a moderate porosity. The precision data reveal new and previously unrealized effects in the form of a field-dependent two-magnon scattering contribution to ΔH_{eff} that is connected with extremely low wave number electromagnetic spin-wave modes and vanishes only in the extreme high-field limit. This signature is particularly clear because the HFE linewidth extrapolates to the expected single-crystal intrinsic values at infinite field. The microstructure also has a signature in the high-field ΔH_{eff} data. For the CS material, one also finds an abrupt increase in the ΔH_{eff} as the field comes within $8\pi M_s/3$ of the high-field bulk manifold band edge. This $8\pi M_s/3$ term corresponds to the maximum dipole field around a pore. The size of the increase appears to change with density and hence, porosity.

ACKNOWLEDGMENTS

This work was supported in part by the United States Office of Naval Research, Grant No. N00014-94-1-0096, the U. S. Army Research Office, Grant No. DAAD19-02-1-0197 and No. W911NF-04-1-0247, and the National Science Foundation, Grant No. DMR-0108797. Dr. Jerome J. Green and Dr. Pavel Kabos are acknowledged for helpful discussions. The hipped YIG materials were prepared by G. M. Argentina and Dr. H. Jerrold Van Hook. The CS YIG materials were provided by Trans Tech. Adamstown, Maryland. Kevin R. Smith is acknowledged for a careful reading of the manuscript.

[1] T. Kohane and E. Schlömann, J. Appl. Phys. **39**, 720 (1968).
[2] Q. H. Vrehen, J. Appl. Phys. **40**, 1849 (1969).
[3] C. E. Patton, Phys. Rev. **179**, 352 (1969).
[4] C. E. Patton, J. Appl. Phys. **41**, 1335 (1970).
[5] C. E. Patton, F. Ono, and M. Takahashi, IEEE Trans. Magn. **7**, 760 (1971).
[6] C. E. Patton and T. Kohane, Rev. Sci. Instrum. **43**, 76 (1972).
[7] W. D. Wilber and L. M. Silber, J. Appl. Phys. **63**, 3353 (1988).
[8] H. Moosmüller, K. D. Mckinstry, and C. E. Patton, IEEE Trans. Magn. **25**, 2482 (1990).
[9] K. D. McKinstry, Ph. D. thesis, Colorado State University, 1991.
[10] J. R. Truedson, K. D. McKinstry, P. Kabos, and C. E. Patton, J. Appl. Phys. **74**, 2705 (1993).
[11] V. L. Safonov and H. N. Bertram, Phys. Rev. B **61**, R14893 (2000).
[12] A. Azevedo, A. B. Oliveira, F. M. de Anguiar, and S. M. Rezende, Phys. Rev. B **62**, 5331 (2000).
[13] V. L. Safonov and H. N. Bertram, J. Appl. Phys. **91**, 8653 (2002).
[14] R. D. McMichael, D. J. Twisselmann, and A. Kunz, Phys. Rev. Lett. **90**, 227601 (2003).
[15] A. V. Nazarov, D. Menard, J. J. Green, C. E. Patton, G. M. Argentina, and H. J. Van Hook, J. Appl. Phys. **94**, 7228 (2003).
[16] V. L. Safonov and H. N. Bertram, J. Appl. Phys. **94**, 529 (2003).
[17] U. Hoeppe, *Off-Resonance Relaxation of Uniform Precession Mode in Microwave Ferrites*, 9th International Conference on Ferrites (ICF-9), San Francisco, California, 22–27 August 2004 (unpublished).
[18] R. D. McMichael and P. Krivosik, IEEE Trans. Magn. **40**, 2 (2004).
[19] G. Woltersdorf and B. Heinrich, Phys. Rev. B **69**, 184417 (2004).
[20] A. Yu. Dobin and R. H. Victora, Phys. Rev. Lett. **92**, 25 7204 (2004).
[21] E. Schlömann, Phys. Rev. **182**, 632 (1969).
[22] M. Sparks, *Ferromagnetic Relaxation Theory* (McGraw-Hill, New York, 1964).
[23] K. Motizuki, M. Sparks, and P. E. Seiden, Phys. Rev. **140**, 972 (1965).
[24] E. Schlömann and R. I. Joseph, *Spin Waves and Magnetoelastic Waves* (Raytheon Technical Report R-68, 1968).
[25] B. Lax and K. J. Button, *Microwave Ferrites and Ferrimagnetics* (McGraw-Hill, New York, 1962).
[26] C. E. Patton, Czech. J. Phys., Sect. B **B26**, 925 (1976).
[27] M. Sparks, R. Loudon, and C. Kittel, Phys. Rev. **122**, 791 (1961).
[28] C. E. Patton, in *Magnetic Oxides*, edited by D. J. Craik (Wiley, London, 1975), p.575.
[29] P. E. Wigen, Phys. Rev. **133**, A1557 (1964).
[30] C. E. Patton, C. H. Wilts, and F. B. Humphrey, J. Appl. Phys. **38**, 1358 (1967).

Downloaded 07 Jul 2005 to 129.82.31.230. Redistribution subject to AIP license or copyright, see http://jap.aip.org/jap/copyright.jsp

[31]M. Sparks, Phys. Rev. B **1**, 3856 (1970).
[32]M. J. Hurben and C. E. Patton, J. Appl. Phys. **83**, 4344 (1998).
[33]R. Arias and D. L. Mills, J. Appl. Phys. **60**, 7395 (1999).
[34]K. J. Harte, J. Appl. Phys. **39**, 1503 (1968).
[35]J. F. Cochran, R. W. Qiao, and B. Heinrich, Phys. Rev. B **39**, 4399 (1989).
[36]B. Heinrich and J. F. Cochran, J. Appl. Phys. **57**, 3690 (1985).
[37]P. Kabos and C. E. Patton, Appl. Phys. Lett. **47**, 759 (1985).

Downloaded 07 Jul 2005 to 129.82.31.230. Redistribution subject to AIP license or copyright, see http://jap.aip.org/jap/copyright.jsp